ELSEVIER

Contents lists available at ScienceDirect

Earth and Planetary Science Letters

journal homepage: www.elsevier.com/locate/epsl



Ediacaran-Ordovician tectonic and geodynamic drivers of Great Unconformity exhumation on the southern Canadian Shield



Barra A. Peak^{a,*}, Rebecca M. Flowers^a, Francis A. Macdonald^b

- ^a Department of Geological Sciences, University of Colorado, Boulder, CO 80309, USA
- ^b Earth Science Department, University of California, Santa Barbara, CA 93106, USA

ARTICLE INFO

Article history: Received 27 February 2023 Received in revised form 14 June 2023 Accepted 24 July 2023 Available online xxxx Editor: R. Bendick

Keywords: thermochronology erosion tectonics geodynamics Laurentia

ABSTRACT

The Great Unconformity erosion surface between Paleozoic sedimentary rocks and Archean-Proterozoic basement has been related to erosion occurring during Snowball Earth glaciations, eustatic sea level fluctuations, and a range of tectonic and/or geodynamic mechanisms. Each class of mechanism predicts distinct timing and spatial patterns of exhumation. Snowball Earth glacial erosion is limited to 717-635 Ma and concentrated in narrow ice streams on continental margins. Sea-level related erosion is unconstrained in time but also spatially limited to continental margins. Tectonic and geodynamic mechanisms, in contrast, can result in exhumation distributed more broadly in time and space. We combine new zircon and apatite (U-Th)/He thermochronology data (ZHe, AHe) with independent paleodepth information from a continental interior location in southeastern Ontario, Canada to constrain the timing, magnitude, and regional pattern of exhumation associated with the Great Unconformity along a \sim 650 km-long transect across the southern Canadian Shield. Here, the unconformity is defined by Middle Ordovician carbonates atop Archean-Proterozoic basement. ZHe analyses for seven basement samples display a range of dates from 960 \pm 20 Ma to 37.5 \pm 0.9 Ma that correlate negatively with radiation damage. AHe dates are ~300-200 Ma and generally consistent across samples regardless of radiation damage. Independent evidence supports emplacement of both the 590 +2/-1 Ma Grenville dikes and the 577 \pm 1 Ma Callander Complex in the study region at depths >6 km. The combined data require ≥6 km of exhumation between ca. 590-577 Ma and 470 Ma in the middle of our transect, with multi-km erosion up to \geq 5 km elsewhere in the study area, well after the $\it ca.$ 717-635 Ma Snowball Earth glaciations. These outcomes expand the spatial extent of an Ediacaran to early-Paleozoic exhumation signal previously inferred elsewhere across the Shield to \sim 1.1 million km 2 . Thick Ediacaran successions on the Laurentian margins are complementary depositional signals of this erosion. The enormous spatial extent of Great Unconformity exhumation across the continental interior of the Canadian Shield is incompatible with glacial erosion and eustatic sea-level change as the primary causes. Instead, we attribute exhumation to tectonic and geodynamic mechanisms, which may include isostatic rebound, dynamic topography, plume activity associated with the Central Iapetus Magmatic Province, rifting during opening of the Iapetus Ocean, and development of the Transcontinental Arch.

© 2023 Elsevier B.V. All rights reserved.

1. Introduction

The "Great Unconformity," or basal Phanerozoic unconformity, is a ubiquitous feature across North America visible as the nonconformable contact between Archean-Proterozoic igneous and metamorphic rocks and overlying Phanerozoic sedimentary rocks. The vast time gap represented by the Great Unconformity – over a billion years of Earth history in some locations – and its broad coinci-

dence with the breakup of Rodinia, assembly of Gondwana, Snowball Earth glaciations, putative oxygenation of the deep oceans, and Cambrian Explosion of biological diversity, have made this feature and the exhumation mechanisms contributing to its formation compelling objects of study. Here, we refer to exhumation—the displacement of rocks with respect to Earth's surface (England and Molnar, 1990)—that exposed basement rocks at the surface before deposition of Phanerozoic sedimentary rocks to form the Great Unconformity as "Great Unconformity exhumation." A related term, "surface uplift" ("uplift" for the remainder of the paper) refers to the vertical displacement of Earth's surface with respect to the Earth's geoid (England and Molnar, 1990). Uplift creates conditions

^{*} Corresponding author.

E-mail address: barra.peak@colorado.edu (B.A. Peak).

conducive to exhumation. Hypothesized mechanisms for Great Unconformity exhumation include glacial erosion during global Snowball Earth events (e.g., Keller et al., 2019; McDannell et al., 2021; McDannell and Keller, 2022), eustatic sea-level change (e.g. Miall, 2016), and tectonic and geodynamically-induced uplift and subsequent erosion (e.g., Flowers et al., 2020; Sturrock et al., 2021; Peak et al., 2021; Macdonald et al., 2022). These mechanisms have been invoked in different locations across North America.

The hypotheses for Great Unconformity exhumation predict distinct timing and spatial patterns of exhumation. Glacial erosion during Cryogenian Snowball Earth events would have caused exhumation concentrated on continental margins limited in time to 717-635 Ma (Macdonald et al., 2022). Eustatic sea-level change is also expected to focus erosion along coastlines (e.g. Bruun, 1988), but unlike Snowball Earth erosion, would not be limited to the Cryogenian. Spatially, erosion driven by eustatic fluctuations is focused along shorelines as the transgressive shoreface system shifts landward (Bruun, 1988). Different tectonic and mantle geodynamic uplift processes can account for exhumation on continental margins and across continental interiors. Tectonic and geodynamic mechanisms elevate the continental topography relative to sea level, thus enabling erosional processes such as river incision to operate more effectively on the landscape (e.g. Braun et al., 2014).

Low-temperature thermochronology provides an opportunity to discriminate among these proposed mechanisms by better constraining the timing, magnitude, and spatial patterns of Great Unconformity exhumation (e.g., DeLucia et al., 2018; Flowers et al., 2020; McDannell and Keller, 2022; Peak et al., 2021; Sturrock et al., 2021). Here, we use new (U-Th)/He thermochronology data from basement below the Great Unconformity on the southern Canadian Shield, together with multiple geologic constraints, to distinguish between proposed hypotheses, acknowledging that different exhumation mechanisms are not necessarily mutually exclusive. We then compare our outcomes with previous thermochronology datasets from across the Canadian Shield to define broader exhumation patterns and further distinguish among possible mechanisms contributing to the Great Unconformity.

2. Background

2.1. Geologic setting and constraints on timing of Great Unconformity exhumation

Our study region on the southern Canadian Shield is located just north of the Great Lakes in southeastern Ontario, Canada (Fig. 1). This area is comprised of three geologic provinces: the Superior and Southern Provinces in the west, composed of Archean and Paleoproterozoic terranes, and the Grenville Province to the east, made up of Proterozoic accreted arc terranes (Percival and Easton, 2007; Fig. 1). The Southern Province is much smaller than the Superior Province and since the period of accretion is irrelevant for the purposes of this study, we refer only to the Superior Province for the remainder of the paper. The region underwent *ca*. 1110-1080 Ma extension and magmatism associated with the Midcontinent Rift, and ca. 1090-980 Ma shortening and crustal thickening associated with the Grenville Orogeny (Percival and Easton, 2007). Some of the region may have been buried by Grenvilleage foreland basins that were later removed; parts of these basins are preserved in the subsurface to the south (e.g., Moecher et al., 2018). After the Grenville Orogeny, the region experienced relative quiescence interrupted from ca. 590-570 Ma by plutonism, emplacement of the Grenville Dike Swarm and Callander Complex (e.g., Kamo et al., 1995), and the opening of the Ottawa-Bonnechere Graben (e.g., Bleeker et al., 2011).

The opening of the Iapetus Ocean followed by dynamic subsidence associated with the Taconic Orogeny (e.g. Coakley and Gurnis, 1995) led to deposition of mixed siliciclastic and carbonate platform sequences preserved from the Middle Ordovician (*ca.* 470 Ma) onward (e.g. Lavoie, 2019; Miall, 2016) that blanket Proterozoic bedrock and define the Great Unconformity. Oxidized paleoregolith is preserved below the unconformity, indicating deep chemical weathering prior to Ordovician deposition (Di Prisco and Springer, 1991). Conodont alteration index values of 1.5-3 for flatlying Ordovician-Devonian strata in the eastern part of the study area (Fig. 1B) indicate post-Ordovician maximum burial temperatures of <100 °C (Legall et al., 1981).

Existing geologic and geochronologic data in the region provide important constraints on the timing of Great Unconformity exhumation. First, the Grenville Dike Swarm, which has a U-Pb TIMS multigrain bulk zircon date of 590 +2/-1 Ma (Kamo et al., 1995), has an ambient emplacement temperature estimate of 184 \pm 40 °C based on paleomagnetic blocking temperatures, corresponding to depths of ~ 6.5 km (Hyodo et al., 1993). In addition, the Callander Complex, a roughly circular composite pluton (Ferguson and Currie, 1972) including a nepheline syenite with a U-Pb zircon date of 577 \pm 1 Ma (Kamo et al., 1995), has emplacement depth estimates of 6-12 km based on petrological relationships (Ferguson and Currie, 1972). These data for the Grenville Dikes and Callander Complex require extensive exhumation after 590-577 Ma to bring these rocks to the surface prior to Middle Ordovician deposition. Additionally, the ca. 1.85 Ga Sudbury Impact Structure, preserved in the Superior Province in the north-central part of the study area (Fig. 1B), has erosion estimates of 4-6 km since \sim 1.24 Ga based on geobarometry and morphology (Molnár et al., 2001; Pope et al., 2004). Exhumation of the Sudbury Impact Structure, the Grenville Dikes, and the Callander Complex may have occurred at the same time after 590-577 Ma.

2.2. Previous low-temperature thermochronology on the central and southern Canadian Shield

Previous thermochronology on the southern and central Canadian Shield (Fig. 1A) includes biotite 40Ar/39Ar, zircon and apatite (U-Th)/He (ZHe, AHe), and apatite fission-track (AFT) data. In the central part of our study area, biotite 40Ar/39Ar thermochronology implies that the basement has been cooler than 320-240 °C since 1126 \pm 2 Ma (Culshaw et al., 2004). To the east, biotite 40 Ar/ 39 Ar, ZHe, and AHe data from the Ottawa-Bonnechere Graben rift flank and Ottawa Embayment were used to infer Neoproterozoic exhumation (Hardie et al., 2017), but this study did not resolve Cryogenian versus Ediacaran exhumation. An AFT study across the southern Canadian Shield from eastern Manitoba through Ontario yielded dates that decrease southeastward from \sim 500-140 Ma (Kohn et al., 2005). These dates record Paleozoic burial heating that partially annealed the fission tracks such that the data are insensitive to earlier parts of the thermal history (Kohn et al., 2005). These data are consistent with AFT data presented in Crowley (1991) from the southern Canadian Shield, in which the oldest dates are Cambrian and the dataset primarily records Mesozoic reheating and cooling.

To the west and north of our study area, a number of thermochronology studies have inferred late Neoproterozoic or early Paleozoic cooling and exhumation events. West of our samples, hematite (U-Th)/He and (U-Th)/Ne data from the Gogebic Iron Range suggest cooling from ~150–65 °C between *ca.* 770–550 Ma (Farley and McKeon, 2015). Farther west, basement AFT data near the Williston Basin yield Neoproterozoic to Ordovician AFT dates interpreted to record late Neoproterozoic and Cambro-Ordovician exhumation before Williston Basin deposition, followed by reheating during Phanerozoic burial (Crowley et al., 1985; Crowley and Kuhlman, 1988). This thermal history is verified by AFT data from a different location on the eastern edge of the Williston Basin

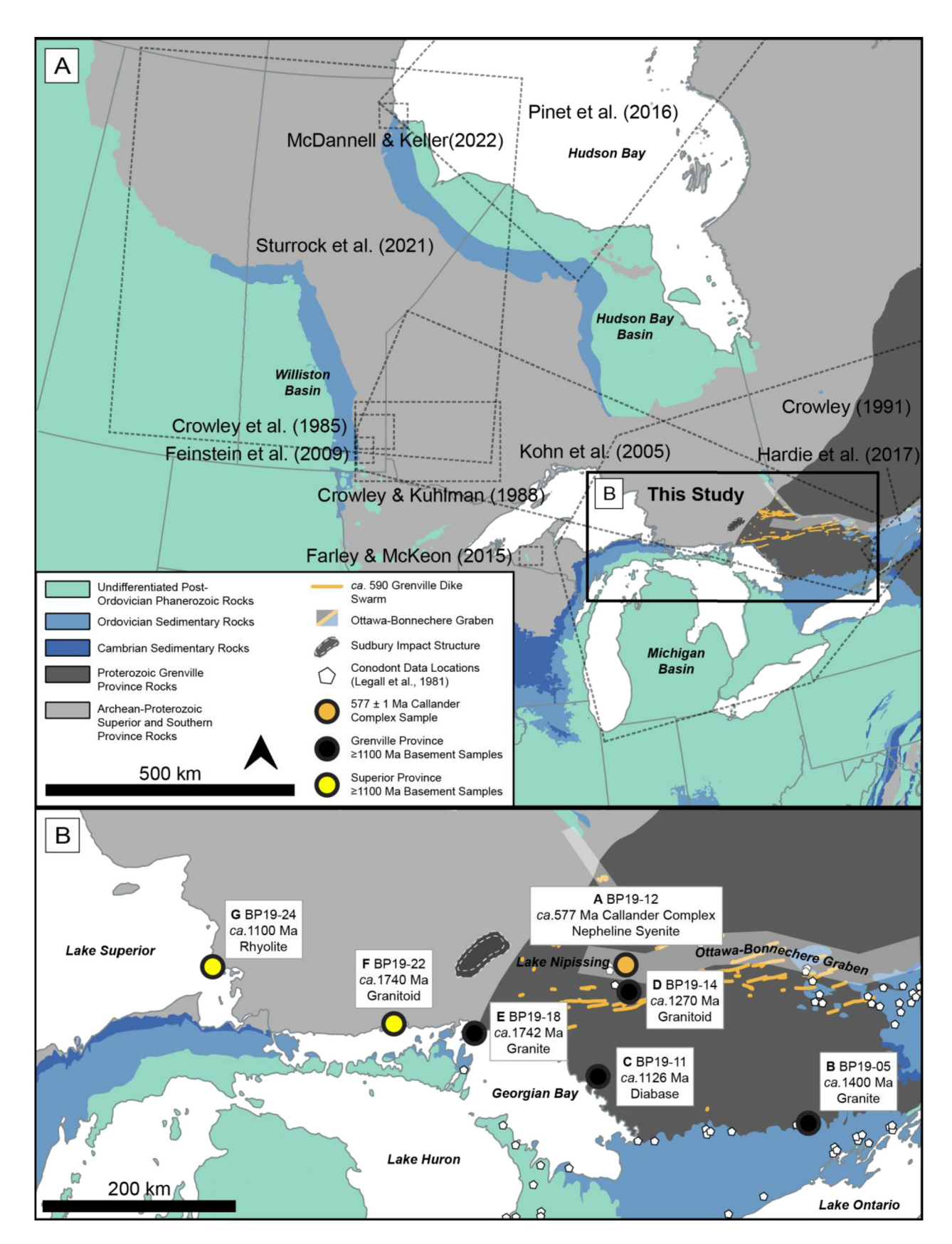


Fig. 1. Simplified geologic map of A) North-Central North America with previous thermochronology study areas marked with dashed outlines and the Ottawa-Bonnechere Graben shown as a white overlay, and B) our study area and sample locations. White pentagons show approximate locations of conodont and acritarch data used to determine maximum Phanerozoic burial temperatures in Legall et al. (1981).

(Feinstein et al., 2009). On the central Canadian Shield, northwest of our study area, AHe data encompassing the eastern edge of the Williston Basin north to the western edge of the Hudson Bay include maximum dates >500 Ma, interpreted to reflect a final stage of Great Unconformity exhumation ≤650 Ma (Sturrock et al., 2021). To the north, ZHe, AHe, and AFT data from two adjacent samples west of Hudson Bay are inferred to reflect Cryogenian exhumation of basement during the Snowball Earth glaciations (McDannell and Keller, 2022). However, AFT data from nearby samples allow the onset of major cooling/exhumation anytime between ∼800-600 Ma, (Pinet et al., 2016), not limited to the Snowball Earth period.

Collectively, these previous studies suggest late Neoproterozoic Great Unconformity exhumation for the central and southeastern Canadian Shield. The timing of this "late" Great Unconformity (Sturrock et al., 2021) is distinct from that inferred from thermochronology studies elsewhere in North America (e.g., DeLucia et al., 2018; Flowers et al., 2020; Peak et al., 2021). Within this Neoproterozoic-Ordovician interval on the Canadian Shield, debate remains regarding whether erosion was predominantly Cryogenian and related to Snowball Earth (McDannell and Keller, 2022), or Ediacaran-Cambrian and related to other mechanisms (Sturrock et al., 2021).

3. (U-Th)/He background and samples

(U-Th)/He thermochronology uses the temperature dependence of He retention in mineral crystals to derive the time-integrated thermal history of a sample. Helium retentivity depends not just on temperature, but on the degree of crystal lattice damage. For minerals with a common thermal history, radiation damage can be proxied by the concentration of parent isotopes weighted for their He productivity as effective uranium concentration, or eU (e.g., Flowers et al., 2009; Shuster et al., 2006). The temperature sensitivity ranges of the zircon and apatite (U-Th)/He systems are <50-220 °C and ~40-115 °C, respectively, depending on accumulated damage (e.g., Flowers et al., 2009; Guenthner et al., 2013). The He diffusion behavior of a crystal as a function of temperature and damage can be simulated using a kinetic model such as the Radiation Damage Accumulation and Annealing Model (RDAAM, Flowers et al., 2009) for apatite and the Zircon Radiation Damage Accumulation and Annealing Model (ZRDAAM, Guenthner et al., 2013) for zircon. Owing to radiation damage effects, positive AHe date-eU correlations and negative ZHe date-eU patterns, are predicted for some thermal histories. Because larger grains are more He retentive than smaller grains, positive correlations between date and mineral grain size are also expected for some thermal histories if other mineral characteristics are the same (Reiners and Farley, 2001). Date-eU and date-grain size patterns can appear "dispersed" due to a variety of factors including grain size, alpha ejection, He implantation, inclusions within the crystal, and parent-nuclide zonation; these effects are described in detail in the supplement.

Seven samples were collected in July 2019 from roadcuts and lake shore exposures across a \sim 650 km WNW-ESE transect of the Grenville and Superior Provinces in southeastern Ontario, Canada (Fig. 1B). Sampling sites were chosen based on proximity to outcrops of the Great Unconformity contact, availability of existing geochronology data, and lithologies likely to contain zircon and apatite. The ca. 577 Ma nepheline syenite of the Callander Complex (BP19-12) was specifically targeted for its younger age and its >6 km emplacement depth, which can be used together with the thermochronology results to help constrain the post-577 Ma thermal history. All other samples are ca. 1.1 Ga or older, with four samples from the Grenville Province and two samples from the Superior Province. All samples are plutonic igneous rocks except for

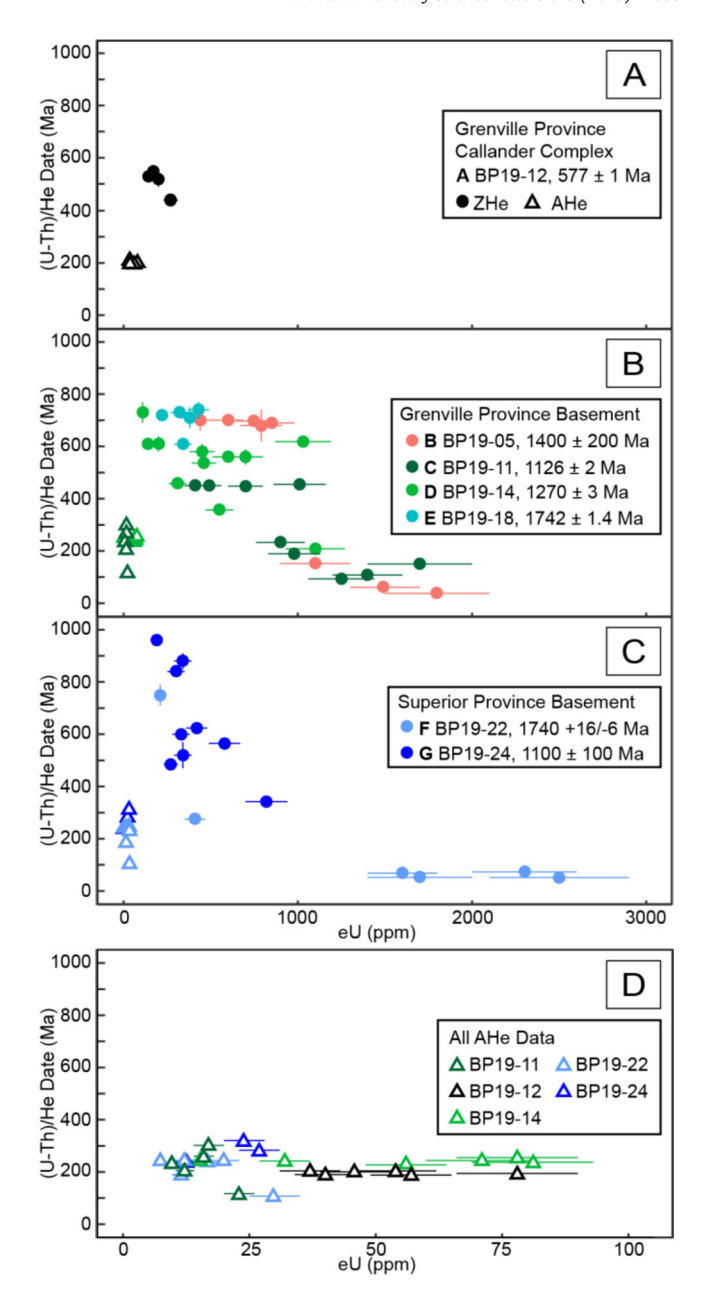


Fig. 2. (U-Th)/He date vs. eU plots for A) Callander Complex sample BP19-12, B) Grenville Province basement samples, C) Superior Province basement samples, and D) AHe analyses for all samples. Note difference in eU scale in panel D. Filled circles denote ZHe analyses and open triangles denote AHe analyses. eU uncertainties are estimated as 15% of eU value. Date uncertainty is 2s propagated total analytical uncertainties on the U, Th, Sm and He measurements (Table S1).

the westernmost sample (BP19-24), which is a shallowly emplaced rhyolite (Swanson-Hysell et al., 2014). ZHe and AHe dates were collected at the University of Colorado Boulder Thermochronology Research and Instrumentation Lab (CU TRalL). Analytical method details are contained in the supplement.

4. Results

ZHe dates were collected for all seven samples (n=4-11/sample) while AHe dates were collected for five samples (n=4-6/sample); two samples from the Grenville Province did not contain apatite. Data are reported in Table S1. Date-eU plots for all samples grouped by geologic province are shown in Fig. 2. The ZHe data for all samples (Fig. 2A-C) exhibit negative date-eU correlations, except for one Grenville Province sample (BP19-18) with a

limited eU range. The ca. 577 Ma Callander Complex sample yields ZHe dates that overlap with or are slightly younger than emplacement, from 550 \pm 20 Ma to 440 \pm 20 Ma across an eU range of \sim 140 to 270 ppm (Fig. 2A). The four Proterozoic basement samples from the Grenville Province together yield a broad range of dates across a wide eU span, with ZHe dates of 740 \pm 30 Ma to 37.5 \pm 0.9 Ma for eU values of \sim 110 to 1800 ppm (Fig. 2B). The two basement samples from the Superior Province yield the oldest ZHe dates of the dataset with four grains >740 Ma, and together span from 960 \pm 20 Ma to 52 \pm 2 Ma over an \sim 190 to 2500 ppm eU range (Fig. 2C). Two samples, a granitoid from the Grenville Province (BP19-14) and the shallow intrusive from the Superior Province (BP19-24), display higher degrees of intrasample dispersion. ZHe dates do not appear to correlate with grain size for any of the samples (Fig. S1).

AHe dates for all samples are broadly similar, with no apparent date-eU correlations and maximum dates that are significantly younger than their zircon counterparts (Fig. 2D). The Callander Complex yields reproducible AHe dates of 188 \pm 7 Ma to 204 \pm 15 Ma over an eU range of $\sim\!\!37$ to 78 ppm. The four Grenville and Superior Province samples with AHe data yield dates from 107 \pm 7 to 320 \pm 10 Ma across an eU range of $\sim\!\!7$ to 81 ppm. There is no correlation between AHe date and grain size, except a weak positive correlation for Grenville sample BP19-11 (Fig. S1).

5. Thermal history interpretation

First-order inferences about the significance of our thermochronology data and the geographic heterogeneity in thermal histories across the study area can be made from the date-eU data patterns. The presence of Neoproterozoic ZHe dates, with the oldest at 960 \pm 20 Ma, shows that our samples record the Neoproterozoic and early Paleozoic thermal history and have not been completely reset by subsequent thermal events. Additionally, the differences in ZHe date-eU trends between samples suggest possible variability in the thermal histories across the study region for example, the westernmost Superior sample yields older dates at the same eU values as the easternmost Grenville sample. In contrast, the good agreement between AHe dates for all samples suggests a shared thermal history in more recent time, with Phanerozoic temperatures hot enough to cause complete apatite He resetting. We can test these interpretations with inverse thermal history modeling.

5.1. Hypothesis testing with thermal history models

5.1.1. Modeling strategy

Each sample was modeled independently to determine consistency with four hypothesized thermal histories derived from non-thermochronologic data and observations (Fig. 3). Several modeling software programs and approaches exist to generate time-temperature (t-T) histories capable of explaining (U-Th)/He thermochronology and other data, but we opted to use HeFTy (Ketcham, 2022) for our primary modeling because it lends itself well to a hypothesis testing approach. Models (individual t-T "paths") are constructed from geologic data and observations in the form of constraint boxes and validated using the thermochronology data. We also modeled our data using the QTQt program (Gallagher, 2012), which uses the Bayesian Information Criterion to converge on the simplest possible thermal history sufficient to explain the thermochronology data. QTQt results and model setup details are given in the supplement.

Each HeFTy model tested 50000 paths generated using a random Monte Carlo approach adhering to the parameters listed in Table S2. To be designated a good or acceptable fit, the combined goodness of fit of a t-T path to all input thermochronology data

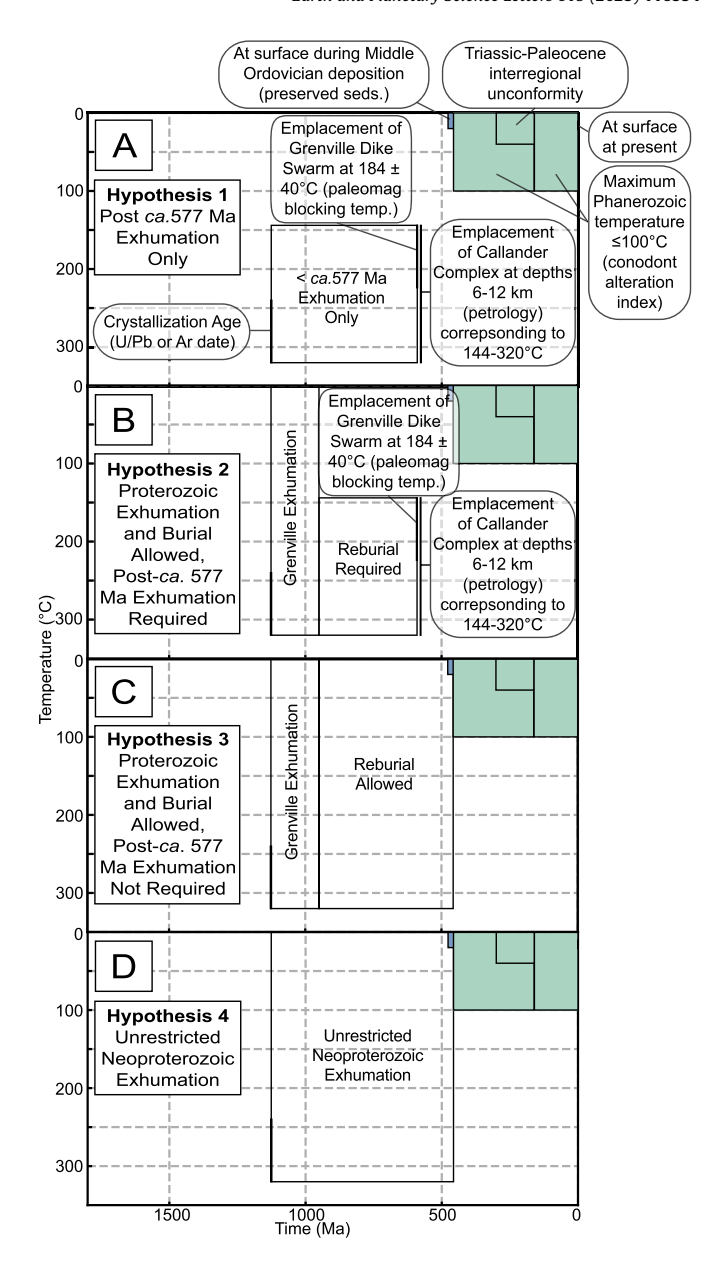


Fig. 3. HeFTy constraint boxes for each hypothesis test. **A) Hypothesis 1: post** *ca.* **577 Ma exhumation only**, tests the hypothesis that most basement cooling/exhumation occurred after *ca.* **577** Ma based on independent information on emplacement of the *ca.* **577** Ma Callander Complex and *ca.* **590** Ma Grenville Dikes at temperatures >144°C. **B) Hypothesis 2: Proterozoic exhumation and burial allowed, post-***ca.* **577 Ma exhumation required** allows cooling/exhumation related to the Grenville Orogeny, subsequent heating/burial to temperatures >144°C, followed by post-*ca.* **577** Ma cooling/exhumation of basement to the surface. **C) Hypothesis 3: Proterozoic exhumation and burial allowed, post-***ca.* **577 Ma exhumation not required,** is the same as Hypothesis **2** but allows final cooling/exhumation of basement to the surface before **577** Ma. **D) Hypothesis 4: Unrestricted Neoproterozoic exhumation,** tests cooling/exhumation-only t-T paths. All models have the same Phanerozoic thermal history constraints (blue and green shaded boxes).

must be \geq 0.5 or \geq 0.05, respectively. The thermochronology data were input using a standard method in which synthetic grains are created by binning the data from each sample by eU and averaging the data values within each bin (Flowers et al., 2022b; Murray et al., 2022; Table S2-S3). The synthetic grain approach accounts for unquantified intrasample date dispersion larger than analytical uncertainties on single grain dates (e.g., Flowers et al., 2022a), such as the dispersion present in the BP19-14 data. The standard error of the uncorrected dates in each bin was applied as the uncorrected date uncertainty of each synthetic grain. Independent geologic data

that informs each sample's thermal history were input using t-T constraint boxes on the allowable t-T space (Fig. 3, Table S2) and are described in Sections 5.1.2 and 5.1.3.

5.1.2. Phanerozoic thermal history constraints

The same Phanerozoic geologic data constraints were applied in all models since these data are regional in scope and the AHe data for all samples is consistent with a shared thermal history across the transect during the Phanerozoic. These constraints are: 1) surface temperatures from 470-444 Ma reflecting Middle Ordovician sedimentary rocks overlying Mesoproterozoic-Ediacaran basement rocks, which locally defines the Great Unconformity, 2) 0-40 °C temperatures from 300-160 Ma reflecting a Triassic-Paleocene interregional unconformity preserved in the Williston Basin (e.g. Butcher et al., 2012) and other Phanerozoic basins to the northwest of our study area (Porter et al., 1982); this unconformity is consistent with regional AFT data interpreted to reflect Mesozoic cooling (Crowley, 1991; Kohn et al., 2005) and was previously shown to be consistent with central Canadian Shield (U-Th)/He data (Sturrock et al., 2021), 3) maximum Phanerozoic temperatures <100°C determined from conodont alteration index classifications across the Grenville Province section of our transect (Legall et al., 1981), and 4) modern average surface temperatures of 0-20 °C.

5.1.3. Precambrian thermal history constraints and hypothesis testing

We developed four different model frameworks to test four different hypotheses for Great Unconformity exhumation (Fig. 3, Table S2). These models are designed to evaluate how sensitive each sample's thermochronologic data are for discriminating among geologically feasible t-T paths. The 577 \pm 1 Ma Callander Complex (sample BP19-12) is younger than the other samples in this study and records only the post-ca. 577 Ma thermal history, therefore only Hypothesis 1 (consistency with only post-ca. 577 Ma exhumation) was tested for this sample. For the six older basement samples, a greater variety of thermal histories are possible because of the longer timescales recorded by these data and thermal history may have varied across the study region. All models include a constraint box representing the timing and temperature of sample formation which differs for each sample; other Precambrian constraint boxes differ between each hypothesis but are consistent across samples (Table S2).

Hypothesis 1, Post-ca. 577 Ma exhumation only (Fig. 3A): These models test the hypothesis that most Great Unconformity exhumation occurred before ca. 577 Ma across the entire study region (after emplacement of the ca. 577 Ma Callander Complex at depth). Farther away from the Callander Complex, this hypothesis is consistent with persistence at high temperatures following the Grenville Orogeny due to structural and foreland basin burial prior to late Neoproterozoic-Cambrian exhumation. To test this in the model framework, all t-T paths are required to remain at temperatures >144 °C before ca. 577 Ma (Fig. 3). The 144 °C temperature is based on the $\it ca.$ 590 Ma Grenville Dike Swarm with 184 \pm 40 $^{\circ}$ C (i.e., 144-224°C) emplacement temperatures estimated from paleomagnetic blocking temperature (Hyodo et al., 1993), and on the Callander Complex nepheline syenite with estimated emplacement depths of 6-12 km from petrological relationships (Ferguson and Currie, 1972), which corresponds to temperatures of 170-320 °C assuming a 20 °C surface temperature and 25 °C/km geotherm. We apply 144°C as the lower temperature bound derived from the Grenville Dike constraint because it is a more direct temperature estimate than that from the Callander Complex, and because as the minimum of the estimated values it is the more conservative

Hypothesis 2, Proterozoic exhumation and burial allowed, post-ca. 577 Ma exhumation required (Fig. 3B): These models test a hypothesis similar to Hypothesis 1 but additionally test an ear-

lier period of exhumation related to Grenville Orogeny deformation (emplacement-950 Ma exploration box), followed by Proterozoic burial to temperatures >144°C (950-577 Ma exploration box). The 950 Ma box boundary is chosen to reflect the known end of Grenville basin development as preserved by the Middle Run Fm in Kentucky and Ohio, USA (Clay et al., 2021). It is possible the southeastern Canadian Shield was buried by a Grenville-age foreland basin similar to those preserved to the south (e.g. Clay et al., 2021; Moecher et al., 2018), but most of this basin, if it existed, was removed prior to Ordovician deposition on the Shield. The minimum reburial temperature is chosen to be consistent with the minimum temperatures required by the Grenville Dike and Callander Complex temperature constraints. Post-577 Ma exhumation to the surface is required after the emplacement of the Grenville Dikes and Callander Complex as in Hypothesis 1.

Hypothesis 3, Proterozoic exhumation and burial allowed, post-ca. 577 Ma exhumation not required (Fig. 3C): These models test the hypothesis that the Grenville Dike and Callander Complex-derived depth constraints are not applicable across the entire study region and allow a final stage of Great Unconformity exhumation to begin before ca. 577 Ma. The model setup is the same as Hypothesis 2 except that it does not require temperatures ≥ 144 °C after 950 Ma.

Hypothesis 4, Unrestricted Neoproterozoic exhumation (Fig. 3D): These models include minimal constraints and test cooling/exhumation-only t-T paths from sample emplacement until Ordovician deposition, with no option to reheat during this interval. The only constraint aside from the Phanerozoic boxes described in Section 5.1.1 is an exploration box from the sample's emplacement age to 457 Ma, which does not restrict when cooling occurred.

5.2. Hypothesis-testing results: substantial post-600 Ma cooling and exhumation

Figs. 4–5 show the model results of each hypothesis test for each sample. Only one hypothesis was tested for the *ca.* 577 Ma Callander Complex sample (Fig. 4), designated as A1. Proterozoic basement sample modeling results are ordered from east to west and labeled as B1, B2, B3, B4, etc. Thermochronology data for individual samples are shown in Figs. 4A and 5B-G with predictions of how each modeled hypothesis reproduces the observed data (Table S4).

A. BP19-12 (ca. 577 Ma Callander Complex nepheline syenite; Fig. 4A): The Callander thermochronology data alone do not provide additional limits on the thermal history beyond the independent geologic data since the set of possible t-T paths fills the entirety of t-T space allowed by the geologic data (Fig. 4A1). However, these results confirm that the thermochronologic and geologic data are consistent with each other, providing a first-order check on our interpretation that the Callander emplacement depth estimate informs the post-577 Ma thermal history.

B. BP19-05 (*ca.* **1400 Ma granite; Fig. 5B):** For this, the easternmost Grenville sample, Hypothesis B1 yields no good- or acceptable-fit paths and Hypothesis B2 returns only a single acceptable-fit path, indicating that the data are difficult to reproduce with these hypotheses and likely inconsistent with sustained temperatures \geq 144°C prior to *ca.*577 Ma. (Fig. 5B1-B2). Given the geographic distance of this sample from the Grenville Dike Swarm and Callander Complex, it is possible that those constraints are not applicable to this sample. All paths yielded by Hypotheses B3 and B4 cool below 130°C after \sim 600 Ma (Fig. 5B3-B4), with the onset of cooling at higher temperatures starting much earlier (\sim 750 Ma) in some cases.

C. BP19-11 (ca. 1126 Ma diabase; Fig. 5C): Hypothesis tests for this Grenville sample yield only acceptable-fit paths indicating some difficulty in reproducing the data, but all models require

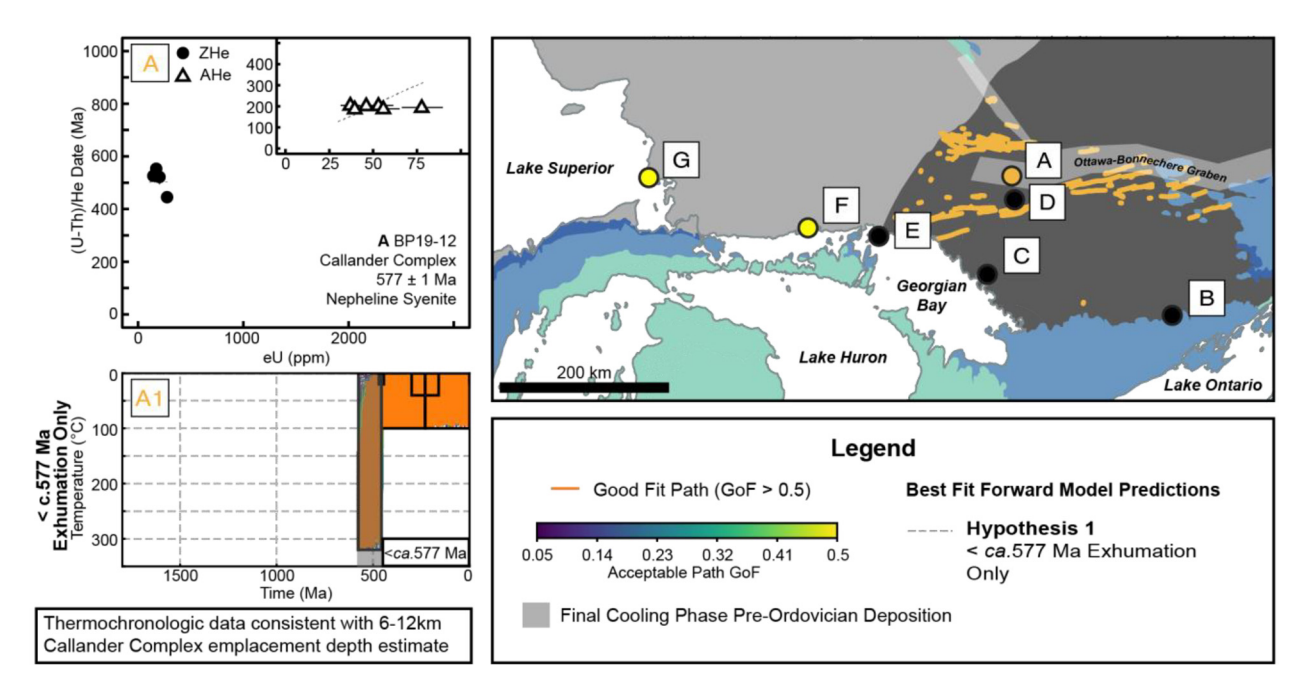


Fig. 4. HeFTy thermal history modeling results for Callander complex sample BP19-12. Sample location is shown on map in orange. A) (U-Th)/He data used to validate models overlain with forward model prediction of data eU range from best-fit inverse model. Date forward model predictions are made with synthetic grains with radii equal to the average grain radius for each sample (Table S4). A1) HeFTy inverse thermal history modeling results. Good-fit paths (goodness of fit (GoF) > 0.5) shown in orange, acceptable fit paths (GoF > 0.05 and < 0.5) shown in gradient from blue to yellow. Gray shaded areas highlight required timing of a final phase of cooling in each model and timing of onset of this cooling period is labeled in the bottom right corner.

a final phase of cooling below 200 °C post \sim 555 Ma (Fig. 5C1-C4), with or without application of the Grenville Dike/Callander emplacement temperature constraints. This outcome is consistent with the proximity (\sim 50-110 km) of BP19-11 to the Grenville Dikes and Callander Complex.

D. BP19-14 (ca. 1270 Ma Powassan Batholith granitoid; Fig. 5D): For this Grenville sample, all good-fit paths yielded by all hypothesis tests, with or without inclusion of the Grenville Dike/Callander emplacement temperature constraints, require final cooling to below $150\,^{\circ}\text{C}$ post $\sim\!600\,\text{Ma}$ (Fig. 5D1-D4). This is compatible with this sample's proximity ($<\!30\,\text{km}$) to the Callander Complex.

E. BP19-18 (ca. 1742 Ma Killarney Complex granite; Fig. 5E): This sample is located within the Grenville Province but is geographically closer to the samples farther west in the Superior Province (Fig. 1B). Model results for Hypotheses E3 and E4 yield good-fit paths that all show a final phase of cooling post \sim 750 Ma, with as much as \sim 130 °C of cooling after 577 Ma (Fig. 5E3-E4). Although the data can also be reproduced by Hypotheses E1 and E2 that require temperatures \geq 144 °C until 577 Ma, the lack of good-fit paths indicates that the data are easier to reproduce well with the lower magnitudes of post-577 Ma cooling allowed by Hypotheses E3 and E4 (Fig. 5E1-E4).

F. BP19-22 (ca. 1740 Ma Cutler Pluton granitoid; Fig. 5F): For this sample in the Superior Province, good-fit paths produced for every hypothesis test cool below $\sim\!200\,^{\circ}\text{C}$ after $\sim\!600\,$ Ma; acceptable-fit paths show a greater range of behavior (Fig. 5F1-F4). Based on the good-fit paths, we interpret this sample's last major phase of Great Unconformity exhumation to occur post-600 Ma.

G. BP19-24 (ca. 1100 Ma rhyolitic intrusive; Fig. 5G): Unlike the other samples, which are slower-cooling intrusive rocks, this sample from Mamainse Point is a shallow intrusive that was emplaced into near-surface conditions (Swanson-Hysell et al., 2014) and therefore requires burial to temperatures hot enough to cause partial He loss from zircon to generate ZHe dates younger than emplacement. Due to this requirement, all hypothesis tests return paths that are essentially identical in requiring Proterozoic reheating >150 °C. At this locality there was likely significant heating

from burial by the overlying Mamainse Point Volcanics and postrift sedimentary rocks (Swanson-Hysell et al., 2014), in addition to structural burial during the Rigolet stage of the Grenville Orogeny (Hodgin et al., 2022) and possible burial by a Grenville foreland basin. Following burial heating, all good-fit paths for all hypothesis tests require post-600 Ma cooling below $\sim\!150\,^{\circ}\text{C}$ (Fig. 5G1-G4), so we interpret the final stage of Great Unconformity exhumation for this sample to be post-600 Ma.

In summary, our HeFTy modeling of the (U-Th)/He data and independent geologic information from the Callander Complex and Grenville Dikes, provide strong evidence for cooling tied to Great Unconformity exhumation from temperatures ≥150 °C to surface temperatures after ${\sim}600$ Ma or ${\sim}577$ Ma. For the Callander Complex model (Fig. 4A1), outcomes are compatible with independent evidence of 6-12 km of exhumation after emplacement at ca. 577 Ma. For three of the five Proterozoic samples in the western \sim 425 km of the transect (BP19-14, -22, -24), all good-fit t-T paths for all hypothesis tests, with or without inclusion of the Callander/Grenville Dike emplacement constraints, require substantial post-600 Ma cooling (at least 150°C) and exhumation. For a fourth sample (BP19-11), all hypothesis tests yield only acceptablefit paths, but all require cooling below at least 200 °C post-600 Ma. The fifth sample (BP19-18) in the middle of the transect permits less, but still substantial (at least 130 °C) cooling and exhumation post-600 Ma. Given that we lack independent evidence that BP19-18 had a different thermal history, we favor a common history of significant post-600 Ma cooling and exhumation across the entire western ~425 km of our transect. A sixth Proterozoic sample (BP19-05) is located \sim 225 km east of the rest of our sample suite. This sample may have undergone as much as 130 °C of cooling post-577 Ma, but this is not required and the sample may have an alternate history. The QTQt modeling results are broadly consistent with these interpretations and suggest that the thermochronology data modeled independently of any other geologic information lack the t-T history resolving power gained when multiple types of data are combined as in our HeFTy models. Full QTQt model setup and discussion are in the supplement.

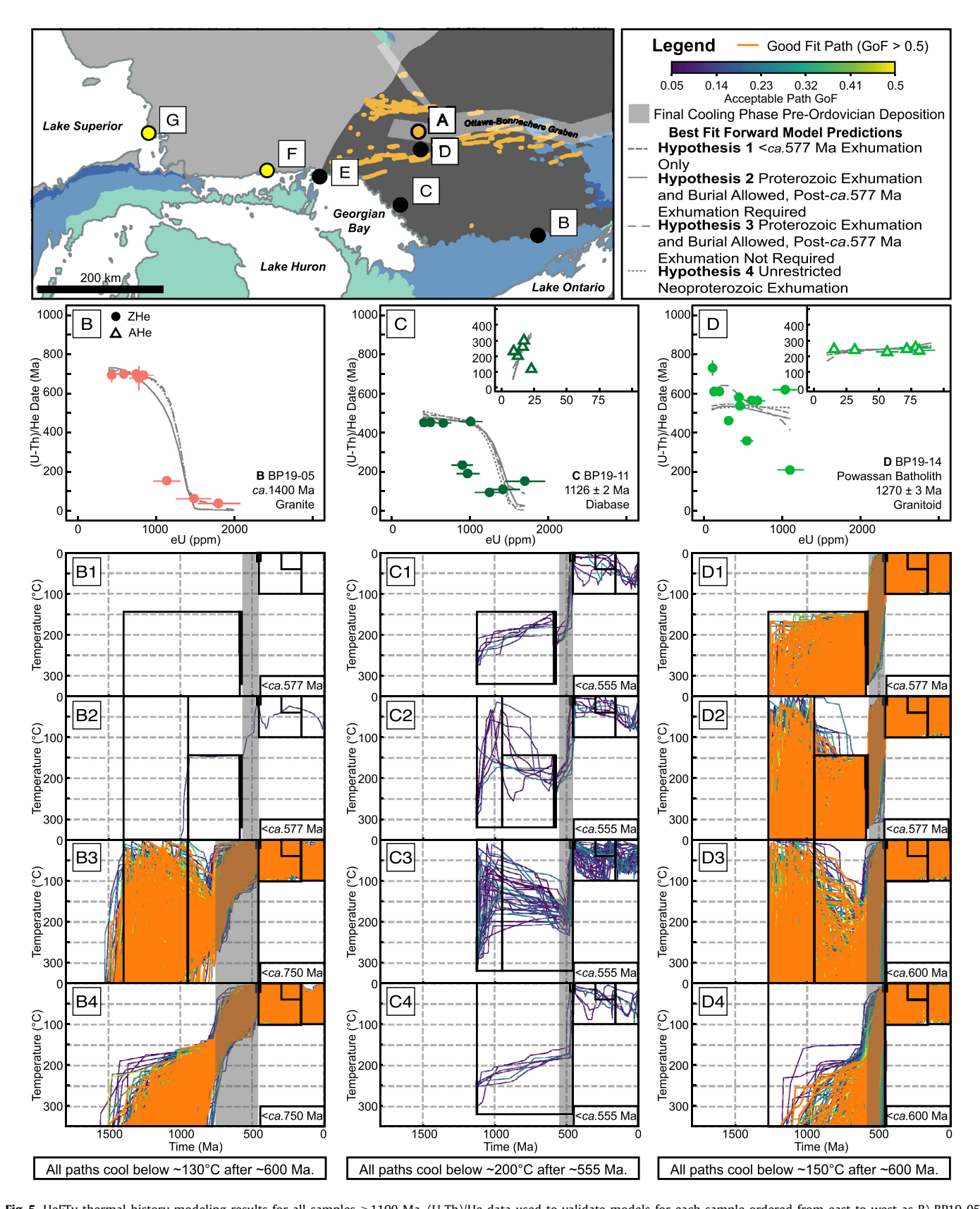


Fig. 5. HeFTy thermal history modeling results for all samples ≥1100 Ma. (U-Th)/He data used to validate models for each sample ordered from east to west as B) BP19-05, C) BP19-11, D) BP19-14, E) BP19-18, F) BP19-22, and G) BP19-24. Data is overlain with forward model predictions for the eU range represented by the data corresponding to the best fit path from each inverse model for that sample. Date forward model predictions are made with synthetic grains with radii equal to the average grain radius for each sample (Table S4). Panels 1-4) HeFTy inverse thermal history results corresponding to each hypothesis test shown in Fig. 3; path legend is the same as Fig. 4. Gray shaded areas highlight required timing of a final phase of cooling in each model and timing of onset of this cooling period is labeled in the bottom right corner of each panel.

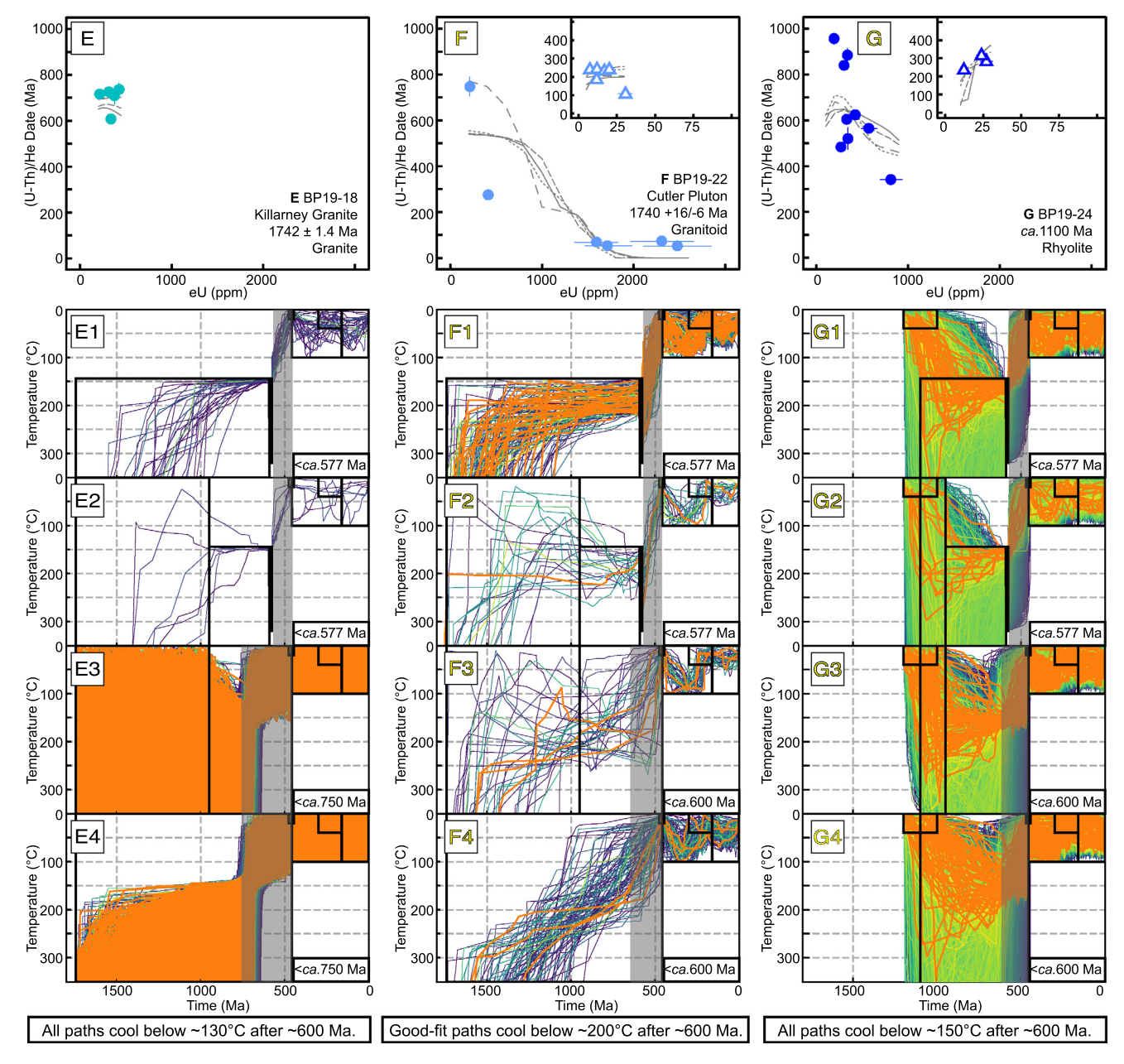


Fig. 5. (continued)

6. Discussion

6.1. Ediacaran-Ordovician exhumation across the southern and central Canadian Shield

The data and associated thermal history models presented here for a transect across the southern Canadian Shield provide evidence for substantial cooling associated with multiple kilometers of exhumation between ca.~600-577 Ma and deposition of Middle Ordovician sedimentary rocks that define the Great Unconformity. The maximum eroded thickness (≥ 6 km) is required in the central part of the transect by the 6-12 km emplacement depth estimates for the ca.~577 Ma Callander Complex (Ferguson and Currie, 1972) and the $184 \pm 40\,^{\circ}\text{C}$ emplacement temperature estimates for the ca.~590 Ma Grenville Dike Swarm (Hyodo et al., 1993). Thermochronologic data for our Proterozoic samples indicate at least $150\,^{\circ}\text{C}$ of cooling for most samples from 600-470 Ma, and all allow at least $130\,^{\circ}\text{C}$ of cooling in this interval. This does

not preclude earlier stages of cooling and exhumation contributing to Great Unconformity exhumation. However, assuming surface temperatures of 0-20°C and a geothermal gradient of 25°C/km, 150 °C of cooling corresponds to 5.2-6 km of exhumation (or 4.4-5.2 km for 130 °C of cooling) from 600-470 Ma. The geothermal gradient may have varied during this time but comparison across continental settings shows $< \sim 10$ °C/km of variation at < 100 km depth, even when considering plume heating effects (e.g., Reston and Morgan, 2004). Assuming a maximum gradient of 35 °C/km results in a minimum exhumation estimate of 3.1-3.7 km for 130 °C and 150°C of cooling, respectively. In the Superior Province, the estimated 4-6 km of erosion for the Sudbury Impact Structure (Molnár et al., 2001; Pope et al., 2004) is compatible with these thermal history interpretations. Our data lack the resolution to resolve different rates of cooling that might be diagnostic of specific exhumation mechanisms, as shown by the disparate range of path behavior from 600-470 Ma (Fig. 4-5).

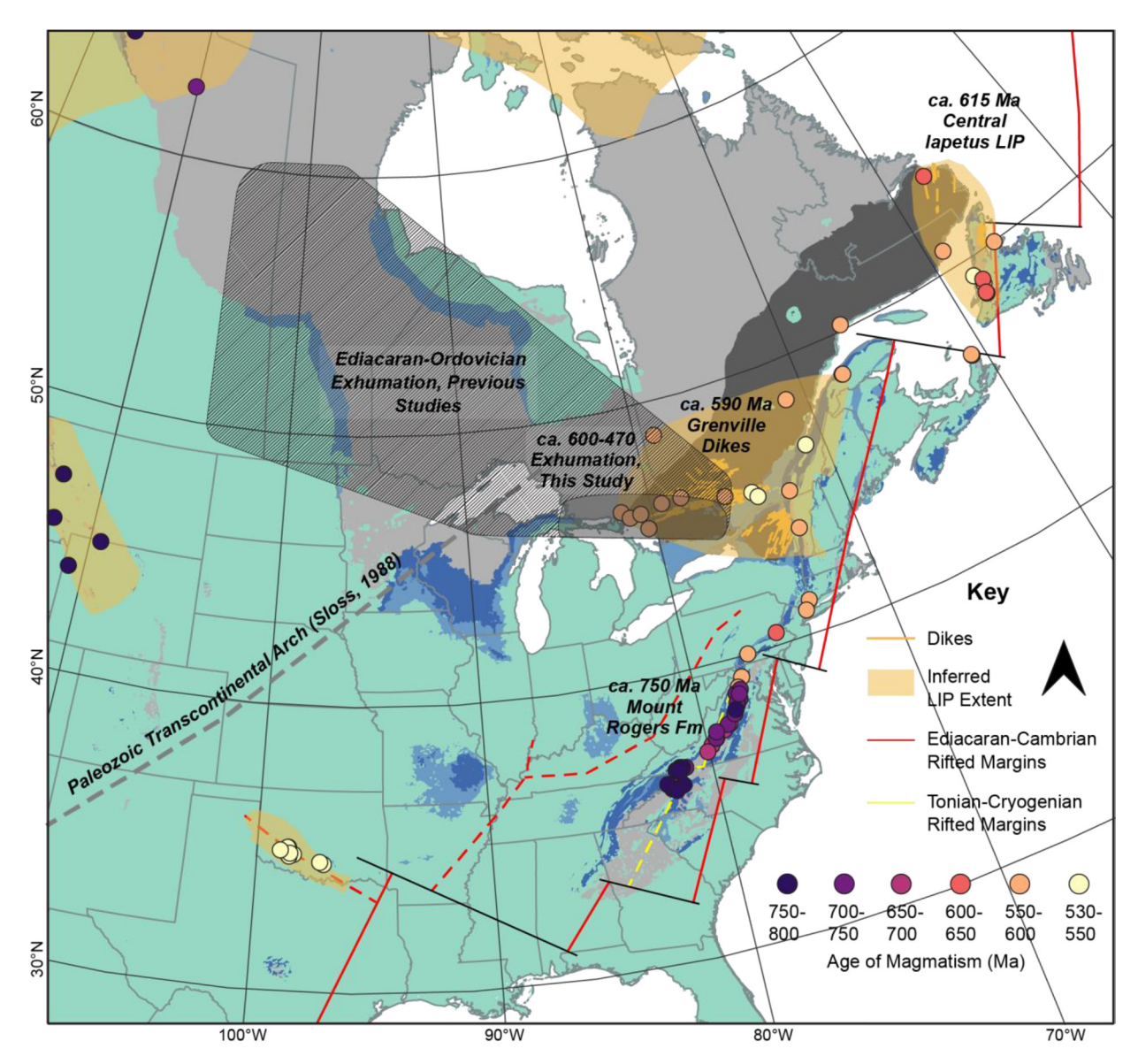


Fig. 6. Map showing spatial extent of Ediacaran-Ordovician exhumation inferred from geologic information, thermochronologic data, and modeling relative to modern topography. Gray transparent overlay: area of this study. Hatched overlay: area of previous low-temperature thermochronology discussed in text. Preserved evidence of tectonic and mantle geodynamic activity that could be contributing to this exhumation signal also shown. Magmatism, faults, and LIP extent after Macdonald et al. (2022). Transcontinental Arch hinge line after Sloss (1988). Geologic map units the same as Fig. 1.

Our results are consistent with previous thermochronology studies in the region and more broadly on the Canadian Shield (Fig. 1A, Section 2.2) that suggest Ediacaran-early Paleozoic basement cooling. This past work interpreted multi-kilometer cooling and exhumation of the basement sometime after 650-600 Ma (e.g. Crowley et al., 1985; Crowley and Kuhlman, 1988; Feinstein et al., 2009; Sturrock et al., 2021). We interpret our (U-Th)/He data to reflect the same signal, extending multi-km Ediacaran-Ordovician Great Unconformity exhumation to cover a roughly 1.1 million km² region of the Canadian Shield (Fig. 6).

This widespread exhumation signature is consistent with sedimentary records on Laurentia's eastern and western margins. Margin sequences preserve thick Tonian and Cryogenian rift-related deposits (Macdonald et al., 2022). However, when adjusted for the long duration of the Cryogenian glaciations, sedimentation rates are low, suggesting little continental erosion during Snowball Earth (e.g., Partin and Sadler, 2016). Margins also host thick Ediacaran-Cambrian successions (Macdonald et al., 2022), that we infer to be the complementary depositional signals to Late Ediacaran-

Cambrian erosion on the Shield. Detrital zircon data from the Ediacaran successions are dominated by Mesoproterozoic zircon originally sourced from the Grenville and Llano uplifts (e.g., Brennan et al., 2021; Zotto et al., 2020). Much of this zircon is likely recycled from Mesoproterozoic foreland basins and Tonian intercontinental basins (Zotto et al., 2020), such as what may have covered the western area of our sample transect. Basin sedimentary strata would have been more erodible than crystalline basement (Flowers and Ehlers, 2018), facilitating erosion.

6.2. Tectonic and geodynamic mechanisms for Ediacaran-Ordovician exhumation on the Canadian Shield

The timing and spatial pattern of Great Unconformity exhumation across the southern and central Canadian Shield is most plausibly explained by geodynamic mechanisms with possible contributions from tectonic events. The extensive footprint of Ediacaranearly Paleozoic exhumation in this area is incompatible with glacial erosion during Snowball Earth, which instead predicts exhumation from 717-635 Ma focused along continental margins or in nar-

row ice-streams based on comparison to modern Antarctic glacial erosion, our closest analog environment (e.g., Abbot et al., 2013; Jamieson et al., 2010). The Canadian Shield exhumation signal is inconsistent with eustatic sea-level change as a dominant mechanism, because this mechanism is also limited to along continental margins as erosional base level shifts due to rising or receding sea levels (e.g., Bruun, 1988; Miall, 2016; Sloss, 1963).

Instead, our work points to tectonic and geodynamic mechanisms to account for the timing, continental interior position, and enormous spatial extent of exhumation. Tectonics and geodynamics are not necessarily independent because tectonic setting can influence mantle flow, and mantle flow can influence crustal processes. Dynamic topography and isostatic rebound are two mantle flow uplift mechanisms (e.g., Mitrovica et al., 2020). Plumes and mantle upwelling can cause uplift on their own (e.g., Friedrich et al., 2018; Pu et al., 2022) and are also commonly associated with extension and resulting rift-flank uplift (e.g., Macdonald et al., 2022). North America likely experienced broad convective upwelling during the Late Tonian-Cambrian breakup of Rodinia, an inference consistent with the occurrence of several coeval large igneous provinces (LIPs) on North America (Macdonald et al., 2022), which have been spatially and geodynamically linked with the position of Large Low Shear-wave Velocity Provinces (LLSVPS; e.g., Burke et al., 2008). Moreover, North America was far from any subduction zones at this time, which are associated with mantle downwelling (e.g., Coakley and Gurnis, 1995). It is likely that a combination of mechanisms resulting from mantle upwelling contributed to the observed up to >5-6 km exhumation signal on the Canadian Shield, though the magnitude of contributions differs.

Mantle-flow induced uplift through dynamic topography or glacio-isostatic rebound may have played a role in uplift during the Ediacaran-Ordovician period of exhumation observed. Dynamic topography can result in elevation change from tens of meters to >1 km and operates over hundreds of kilometers (e.g., Braun, 2010; Mitrovica et al., 2020), such that dynamic topography could have contributed a significant portion of the total exhumation we observe, though its true contribution is difficult to quantify. Glacioisostatic rebound likely impacted the region immediately following the Cryogenian Snowball Earth deglaciations at ca. 660 and 635 Ma, but no ice sheets were present on the modern Canadian Shield during the more-recent Gaskiers and Upper Ediacaran glaciations (Macdonald et al., 2022). Glacio-isostatic rebound has different magnitudes depending on topography and distance from ice sheet epicenters (Mitrovica et al., 2020), but in general predicts elevation changes on the order of 10 s to 100 s of meters over a million-year timescale. However, during the Cryogenian, North America was situated along the equator (Macdonald et al., 2022), and climate models of Snowball Earth predict dry valleys at these latitudes (e.g., Benn et al., 2015) which would have minimized both glacial erosion and glacio-isostatic rebound. Thus, glacio-isostatic rebound is inconsistent with more than a minor role in the observed exhumation signal.

Multiple plumes emplaced at different times in the Ediacaran-Ordovician and their lithospheric effects can explain the cooling signals across the transect. Independent evidence for plumes has been associated with formation of the Ottawa-Bonnechere Graben (Hardie et al., 2017) and opening of the Iapetus Seaway and includes preserved dike swarms, plutonic intrusions such as the Callander Complex, kimberlites, and inferred relationships to LIPs and an LLSVP associated with the *ca.* 615 Ma Central Iapetus Magmatic Province (Robert et al., 2021; Tegner et al., 2019; Fig. 6). Plumes can thermally and chemically modify the lithosphere, leading to density instabilities, lithospheric delamination, and elevation changes at the surface (e.g., Friedrich et al., 2018; O'Connell and Wasserburg, 1972). Elevation changes associated with plumes have

been modeled on the order of 1 km (Peng et al., 2022), a significant contribution.

A well-studied example of continental interior uplift and exhumation from geodynamic causes is the southern African Plateau, which was surrounded by extensional plate boundaries when it underwent Mesozoic-Cenozoic surface uplift, likely due to a combination of mantle upwelling, lithospheric thinning, and lithospheric thermochemical modification (e.g., Braun et al., 2014; Stanley et al., 2015, 2021). The pattern of Ediacaran sedimentation observed in North America and described in Section 6.1 is also similar to the Mesozoic-Cenozoic erosion and deposition pattern in southern Africa, where kilometers of overburden were removed from the continental interior and redeposited along the modern African margins following geodynamically-driven uplift (e.g., Baby et al., 2020; Braun et al., 2014; Stanley et al., 2015; Tinker et al., 2008), suggesting that southern Africa's more-recent uplift and exhumation history is a good analog for the Ediacaran-Ordovician history of the south-central Canadian Shield.

Faulting and tectonically-driven uplift may have also played a role on the Canadian Shield during the Ediacaran-Ordovician. Paleozoic paleo-high development extending across the middle of modern North America, the "Transcontinental Arch" (e.g., Brennan et al., 2021; Sloss, 1988) correlates with the onset of the Neoproterozoic-Cambrian rift-drift transition along the Iapetan margin (Brennan et al., 2021; Macdonald et al., 2022; Robert et al., 2021). The arch could have been accommodated by transform faults that reactivated older basement weaknesses during the Neoproterozoic-Cambrian opening of the Iapetus Ocean (Brennan et al., 2021). Faulting related to rifting, such as the Ottawa-Bonnechere graben in our study area, is also associated with extensive magmatism and dynamic uplift effects. Although the Mid-Continent Rift is just to the west of our study area, the most recent period of fault reactivation is dated at ca. 985 Ma (Hodgin et al., 2022), well before the exhumation signal we observe. By the Ordovician, a subduction margin had developed adjacent to North America (Coakley and Gurnis, 1995), resulting in mantle downwelling associated with subducting slabs, the flooding of North America and conditions favorable to deposition and carbonate precipitation of the Middle Ordovician rocks preserved today.

7. Conclusions

This study presents new zircon and apatite (U-Th)/He thermochronology dates for the southeastern Canadian Shield and uses these data to test hypotheses for large-scale exhumation related to the Great Unconformity. Cooling histories informed by basement rock ZHe, AHe, and independent temperature-time constraints on emplacement of the ca. 590 Ma Grenville Dike Swarm and ca. 577 Ma Callander Complex provide strong evidence for >6 km of exhumation between ca. 577 and 470 Ma in the center of the transect, with as much as ≥ 5 km after ca. 600 Ma across at least the western 425 km. This history is consistent with previous low-temperature thermochronology on the central and southern Canadian Shield (e.g. Crowley et al., 1985; Crowley and Kuhlman, 1988; Feinstein et al., 2009; Sturrock et al., 2021) and we interpret our results and those of these past studies to record the same Ediacaran-early Paleozoic exhumation signal, expanding its footprint to encompass over a million km². This widespread signal is likely a composite of multiple causal mechanisms during this time period. However, based on the spatial pattern of exhumation over the cratonic interior and the predominantly Ediacaran-Ordovician timing of exhumation, we rule out Snowball Earth glacial erosion and eustatic sea level rise as responsible for the signal we observe. Ediacaran-Ordovician exhumation can instead be explained with a combination of geodynamic and tectonic mechanisms similar to the exhumation history inferred for Mesozoic-Cenozoic southern

Africa. Plausible mechanisms include dynamic topography, plume impingement, and faulting associated with opening of the lapetus ocean and development of the Transcontinental Arch.

CRediT authorship contribution statement

Barra A. Peak: Data curation, Investigation, Methodology, Project administration, Resources, Validation, Visualization, Writing – original draft, Writing – review & editing. **Rebecca M. Flowers:** Conceptualization, Funding acquisition, Investigation, Methodology, Project administration, Resources, Supervision, Writing – original draft, Writing – review & editing. **Francis A. Macdonald:** Conceptualization, Funding acquisition, Investigation, Project administration, Resources, Supervision, Writing – original draft, Writing – review & editing.

Declaration of competing interest

The authors declare that they have no known competing financial interests or personal relationships that could have appeared to influence the work reported in this paper.

Data availability

Data and software parameters used are included in the supplementary tables.

Acknowledgements

This work was funded by NSF EAR-1822119 to RMF, NSF EAR-1916698 to FAM, and a CU Boulder Chancellor's Fellowship to BAP. We thank Jim Metcalf for assistance with analytical data acquisition, Sabrina Kainz for assistance with mineral separation, and Rich Ketcham for providing an early version of HeFTy v.2. We thank Sandra Kamo, Wouter Bleeker, Mike Hamilton, and Nick Swanson-Hysell for helpful discussions. We thank Benjamin Gérard and Andrea Stevens Goddard for thoughtful and careful reviews that greatly improved the manuscript.

Appendix A. Supplementary material

Supplementary material related to this article can be found online at https://doi.org/10.1016/j.epsl.2023.118334.

References

- Abbot, D.S., Voigt, A., Li, D., Le Hir, G., Pierrehumbert, R.T., Branson, M., et al., 2013. Robust elements of Snowball Earth atmospheric circulation and oases for life. J. Geophys. Res., Atmos. 118 (12), 6017–6027. https://doi.org/10.1002/jgrd.50540.
- Baby, G., Guillocheau, F., Braun, J., Robin, C., Dall'Asta, M., 2020. Solid sedimentation rates history of the Southern African continental margins: implications for the uplift history of the South African Plateau. Terra Nova 32 (1), 53–65. https:// doi.org/10.1111/ter.12435.
- Benn, D.I., Le Hir, G., Bao, H., Donnadieu, Y., Dumas, C., Fleming, E.J., et al., 2015. Orbitally forced ice sheet fluctuations during the Marinoan Snowball Earth glaciation. Nat. Geosci. 8 (9), 704–707. https://doi.org/10.1038/ngeo2502.
- Bleeker, W., Dix, G., Davison, A., LeCheminant, A., 2011. Tectonic evolution and sedimentary record of the Ottawa-Bonnechere Graben: examining the Precambrian and Phanerozoic history of magmatic activity, Faulting and sedimentation. In: Proceedings of Geological Association of Canada-Mineralogical Association of Canada, pp. 25–27.
- Braun, J., 2010. The many surface expressions of mantle dynamics. Nat. Geosci. 3, 825–833. https://doi.org/10.1038/ngeo1020.
- Braun, J., Guillocheau, F., Robin, C., Baby, G., Jelsma, H., 2014. Rapid erosion of the Southern African Plateau as it climbs over a mantle superswell. J. Geophys. Res., Solid Earth 119, 6093–6112. https://doi.org/10.1002/2014JB010998.
- Brennan, D.T., Mitchell, R.N., Spencer, C.J., Murphy, J.B., Li, Z.X., 2021. A tectonic model for the Transcontinental Arch: progressive migration of a Laurentian drainage divide during the Neoproterozoic–Cambrian Sauk Transgression. Terra Nova 33 (4), 430–440. https://doi.org/10.1111/ter.12528.

- Bruun, P., 1988. The Bruun Rule of Erosion by sea-level rise: a discussion on large-scale two- and three-dimensional usages. J. Coast. Res. 4 (4), 627–648.
- Burke, K., Steinberger, B., Torsvik, T.H., Smethurst, M.A., 2008. Plume Generation Zones at the margins of Large Low Shear Velocity Provinces on the core-mantle boundary. Earth Planet. Sci. Lett. 265 (1–2), 49–60. https://doi.org/10.1016/j.epsl. 2007.09.042
- Butcher, G.S., Kendall, A.C., Boyce, A.J., Millar, I.L., Andrews, J.E., Dennis, P.F., 2012. Age determination of the Lower Watrous red-beds of the Williston Basin, Saskatchewan, Canada. Bull. Can. Pet. Geol. 60 (4), 227–238. https://doi.org/10.2113/gscpgbull.60.4.227.
- Clay, J.M., Moecher, D.P., Bowersox, J.R., 2021. Detrital zircon U-Pb geochronology of the Precambrian Middle Run Formation (Eastern North America Basement): implications for Grenvillian foreland basin evolution and Midcontinent Rifting. Precambrian Res. 364, 106332. https://doi.org/10.1016/j.precamres.2021.106332.
- Coakley, B., Gurnis, M., 1995. Far-field tilting of Laurentia during the Ordovician continent. J. Geophys. Res. 100, 6313–6327.
- Crowley, K.D., 1991. Thermal history of Michigan Basin and southern Canadian Shield from apatite fission track analysis. J. Geophys. Res. 96 (B1), 697–711. https://doi.org/10.1029/90JB02174.
- Crowley, K.D., Kuhlman, S.L., 1988. Apatite thermochronometry of Western Canadian Shield: implications for origin of the Williston basin. Geophys. Res. Lett. 15 (3), 221–224.
- Crowley, K.D., Ahern, J.L., Naeser, C.W., 1985. Origin and epeirogenic history of the Williston Basin: evidence from fission-track analysis of apatite. Geology 13 (9), 620–623. https://doi.org/10.1130/0091-7613(1985)13<620:OAEHOT>2.0.CO;2.
- Culshaw, N.G., Corrigan, D., Ketchum, J.W.F., Wallace, P., Wodicka, N., 2004. Precambrian geology, Parry Sound area, Ontario Geological Survey, Preliminary Map P. 35500, scale 1:50 000.
- DeLucia, M.S., Guenthner, W.R., Marshak, S., Thomson, S.N., Ault, A.K., 2018. Thermochronology links denudation of the Great Unconformity surface to the supercontinent cycle and snowball Earth. Geology 46 (2), 167–170. https://doi.org/10.1130/G39525.1.
- England, P., Molnar, P., 1990. Surface uplift, uplift of rocks, and exhumation of rocks. Geology 18 (12), 1173–1177. https://doi.org/10.1130/0091-7613(1990) 018<1173;SUUORA>2.3.CO;2.
- Farley, K.A., McKeon, R., 2015. Radiometric dating and temperature history of banded iron formation-associated hematite, Gogebic iron range, Michigan, USA. Geology 43 (12), 1083–1086. https://doi.org/10.1130/G37190.1.
- Feinstein, S., Kohn, B., Osadetz, K., Everitt, R., O'Sullivan, P., 2009. Variable Phanerozoic thermal history in the Southern Canadian Shield: evidence from an apatite fission track profile at the Underground Research Laboratory (URL), Manitoba. Tectonophysics 475 (1), 190–199. https://doi.org/10.1016/j.tecto.2009.01.016.
- Ferguson, J., Currie, K.L., 1972. The geology and petrology of the alkaline carbonatite complex at Callander Bay, Ontario. Bull., Geol. Surv. Can. 217.
- Flowers, R.M., Zeitler, P.K., Danišík, M., Reiners, P.W., Gautheron, C., Ketcham, R.A., et al., 2022a. (U-Th)/He chronology: Part 1. Data, uncertainty, and reporting. Geol. Soc. Am. Bull. Spec. Vol., Reporting 1 (April), 20. https://doi.org/10.1130/B36266. 1/5590022/b36266.pdf.
- Flowers, R.M., Ketcham, R.A., Enkelmann, E., Gautheron, C., Reiners, P.W., Metcalf, J.R., et al., 2022b. (U-Th)/He chronology: Part 2. Considerations for evaluating, integrating, and interpreting conventional individual aliquot data. Geol. Soc. Am. Bull. Spec. Vol., Reporting.
- Flowers, R.M., Ehlers, T.A., 2018. Rock erodibility and the interpretation of low-temperature thermochronologic data. Earth Planet. Sci. Lett. 482, 312–323. https://doi.org/10.1016/j.epsl.2017.11.018.
- Flowers, Rebecca M., Ketcham, R.A., Shuster, D.L., Farley, K.A., 2009. Apatite (U-Th)/He thermochronometry using a radiation damage accumulation and annealing model. Geochim. Cosmochim. Acta 73 (8), 2347–2365. https://doi.org/10.1016/j.gca.2009.01.015.
- Flowers, Rebecca M., Macdonald, F.A., Siddoway, C.S., Havranek, R., 2020. Diachronous development of Great Unconformities before Neoproterozoic Snowball Earth. Proc. Natl. Acad. Sci., 1–9. https://doi.org/10.1073/pnas.1913131117.
- Friedrich, A.M., Bunge, H.P., Rieger, S.M., Colli, L., Ghelichkhan, S., Nerlich, R., 2018. Stratigraphic framework for the plume mode of mantle convection and the analysis of interregional unconformities on geological maps. Gondwana Res. 53, 159–188. https://doi.org/10.1016/j.gr.2017.06.003.
- Gallagher, K., 2012. Transdimensional inverse thermal history modeling for quantitative thermochronology. J. Geophys. Res., Solid Earth 117 (2), 1–16. https://doi.org/10.1029/2011JB008825.
- Guenthner, W.R., Reiners, P.W., Ketcham, R.A., Nasdala, L., Giester, G., 2013. Helium diffusion in natural zircon: radiation damage, anisotropy, and the interpretation of zircon (U-TH)/He thermochronology. Am. J. Sci. 313 (3), 145–198. https://doi.org/10.2475/03.2013.01.
- Hardie, R.A., Schneider, D.A., Garver, J.I., 2017. (U-Th)/he thermochronology of the ottawa embayment, eastern Canada: the temperature-time history of an ancient, intracratonic rift basin. J. Geol. 125 (6), 659–680. https://doi.org/10.1086/ 693859.
- Hodgin, E.B., Swanson-Hysell, N.L., DeGraff, J.M., Kylander-Clark, A.R.C., Schmitz, M.D., Turner, A.C., et al., 2022. Final inversion of the Midcontinent Rift during the Rigolet Phase of the Grenvillian Orogeny. Geology 50 (5), 547–551. https://doi.org/10.1130/G49439.1.

- Hyodo, H., York, D., Dunlop, D.J., 1993. Tectonothermal history in the Mattawa area, Ontario, Canada, deduced from paleomagnetism and 40Ar/39Ar dating of a Grenville dike. J. Geophys. Res. 98 (B10). https://doi.org/10.1029/93jb01555.
- Jamieson, S.S.R., Sugden, D.E., Hulton, N.R.J., 2010. The evolution of the subglacial landscape of Antarctica. Earth Planet. Sci. Lett. 293 (1–2), 1–27. https://doi.org/ 10.1016/j.epsl.2010.02.012.
- Kamo, S.L., Krogh, T.E., Kumarapeli, P.S., 1995. Age of the Grenville dyke swarm, Ontario - Quebec: implications for the timing of lapetan rifting. Can. J. Earth Sci. 32 (3), 273–280. https://doi.org/10.1139/e95-022.
- Keller, C.B., Husson, J.M., Mitchell, R.N., Bottke, W.F., Gernon, T.M., Boehnke, P., et al., 2019. Neoproterozoic glacial origin of the Great Unconformity. Proc. Natl. Acad. Sci. 116 (4), 1136–1145. https://doi.org/10.1073/pnas.1804350116.
- Ketcham, R.A., 2022. HeFty.
- Kohn, B.P., Gleadow, A.J.W., Brown, R.W., Gallagher, K., Lorencak, M., Noble, W.P., 2005. Visualizing thermotectonic and denudation histories using apatite fission track thermochronology. Rev. Mineral. Geochem. 58, 527–565. https://doi.org/10. 2138/rmg.2005.58.20.
- Lavoie, D., 2019. The Cambrian-Devonian Laurentian Platforms and Foreland Basins in Eastern Canada. The Sedimentary Basins of the United States and Canada, second edition. Elsevier B.V.
- Legall, F.D., Barnes, C.R., Macqueen, R.W., 1981. Thermal maturation, burial history and hotspot development, Paleozoic strata of southern Ontario-Quebec, from conodont and acritarch colour alteration studies. Bull. Can. Pet. Geol. 29 (4), 492–539.
- Macdonald, F.A., Yonkee, W.A., Flowers, R.M., Swanson-Hysell, N.L., 2022. Neoproterozoic of Laurentia. In: Laurentia: Turning Points in the Evolution of a Continent. Geol. Soc. Am. Mem. 220, 331–380. https://doi.org/10.1130/2022.1220(19).
- McDannell, K.T., Keller, C.B., 2022. Cryogenian glacial erosion of the central Canadian Shield: the "late" Great Unconformity on thin ice. Geology 50 (12), 1336–1340. https://doi.org/10.1130/g50315.1.
- McDannell, K.T., Keller, C.B., Guenthner, W.R., Zeitler, P.K., Shuster, D.L., 2021. Thermochronologic constraints on the origin of the Great Unconformity. Proc. Natl. Acad. Sci. PrePrint.
- Miall, A.D., 2016. The valuation of unconformities. Earth-Sci. Rev. 163, 22–71. https://doi.org/10.1016/j.earscirev.2016.09.011.
- Mitrovica, J.X., Austermann, J., Coulson, S., Creveling, J.R., Hoggard, M.J., Jarvis, G.T., Richards, F.D., 2020. Dynamic topography and ice age paleoclimate. Annu. Rev. Earth Planet. Sci. 48, 585–621. https://doi.org/10.1146/annurev-earth-082517-010225.
- Moecher, D.P., Bowersox, J.R., Hickman, J.B., 2018. Zircon U-Pb geochronology of two basement cores (Kentucky, USA): implications for late mesoproterozoic sedimentation and tectonics in the eastern midcontinent. J. Geol. 126 (1), 25–39. https://doi.org/10.1086/694825.
- Molnár, F., Watkinson, D.H., Jones, P.C., 2001. Multiple hydrothermal processes in footwall units of the North Range, Sudbury Igneous Complex, Canada, and implications for the genesis of vein-type Cu-Ni-PGE deposits. Econ. Geol. 96 (7), 1645–1670. https://doi.org/10.2113/gsecongeo.96.7.1645.
- Murray, K.E., Goddard, A.L.S., Abbey, A.L., Wildman, M., 2022. Thermal history modeling techniques and interpretation strategies: applications using HeFTy. Geosphere 18 (5), 1622–1642. https://doi.org/10.1130/GES02500.1.
- O'Connell, R.J., Wasserburg, G.J., 1972. Dynamics of submergence and uplift of a sedimentary basin underlain by a phase-change boundary. Rev. Geophys. 10 (1), 335–368. https://doi.org/10.1029/RG010i001p00335.
- Partin, C.A., Sadler, P.M., 2016. Slow net sediment accumulation sets snowball Earth apart from all younger glacial episodes. Geology 44 (12), 1019–1022. https://doi.org/10.1130/G38350.1.
- Peak, B.A., Flowers, R.M., Macdonald, F.A., Cottle, J.M., 2021. Zircon (U-Th)/He thermochronology reveals pre-Great Unconformity paleotopography in the Grand Canyon region, USA. Geology 49 (12), 1462–1466. https://doi.org/10.1130/G49116.1.
- Peng, L., Liu, L., Liu, L., 2022. The fate of delaminated cratonic lithosphere. Earth Planet. Sci. Lett. 594, 117740. https://doi.org/10.1016/j.epsl.2022.117740.

- Percival, J.A., Easton, R.M., 2007. Geology of the Canadian shield in Ontario: an update. Ontario Geological Survey Open File Report 6196, Geological Survey of Canada Open File 5511, Ontario Power Generation Report 06819-REP-01200-10158-R00. Retrieved from http://geoscan.ess.nrcan.gc.ca/cgi-bin/starfinder/0?path=geoscan.fl&id=fastlink&pass=&search=R*3D223891&format=FLFULL.
- Pinet, N., Kohn, B.P., Lavoie, D., 2016. The ups and downs of the Canadian Shield: 1- preliminary results of apatite fission track analysis from Hudson Bay region. GSC, Open File 8110. p. 59.
- Pope, K.O., Kieffer, S.W., Ames, D.E., 2004. Empirical and theoretical comparisons of the Chicxulub and Sudbury impact structures. Meteorit. Planet. Sci. 39 (1), 97–116. https://doi.org/10.1111/j.1945-5100.2004.tb00052.x.
- Porter, J.W., Price, R.A., McCrossan, R.G., 1982. The western Canada sedimentary basin. Philos. Trans. R. Soc. Lond. 305, 169–192.
- Di Prisco, G., Springer, J.S., 1991. The Precambrian-Paleozoic unconformity and related mineralization in southeastern Ontario. Ontario Geological Survey Open File Report 5751
- Pu, J.P., Macdonald, F.A., Schmitz, M.D., Rainbird, R.H., Bleeker, W., Peak, B.A., et al., 2022. Emplacement of the Franklin large igneous province and initiation of the Sturtian Snowball Earth. Sci. Adv. 8 (47), eadc9430. https://doi.org/10.1126/ sciadv.adc9430.
- Reiners, P.W., Farley, K.A., 2001. Influence of crystal size on apatite (U-Th)/He thermochronology: an example from the Bighorn Mountains, Wyoming. Earth Planet. Sci. Lett. 188 (3-4), 413-420. https://doi.org/10.1016/S0012-821X(01) 00341-7
- Reston, T.J., Morgan, J.P., 2004. Continental geotherm and the evolution of rifted margins. Geology 32 (2), 133–136. https://doi.org/10.1130/G19999.1.
- Robert, B., Domeier, M., Jakob, J., 2021. On the origins of the lapetus ocean. Earth-Sci. Rev. 221, 103791. https://doi.org/10.1016/j.earscirev.2021.103791.
- Shuster, D.L., Flowers, R.M., Farley, K.A., 2006. The influence of natural radiation damage on helium diffusion kinetics in apatite. Earth Planet. Sci. Lett. 249 (3–4), 148–161. https://doi.org/10.1016/j.epsl.2006.07.028.
- Sloss, L.L., 1963. Sequences in the Cratonic Interior of North America. Geol. Soc. Am. Bull. 74. 93–114.
- Sloss, L.L., 1988. Tectonic evolution of the craton in Phanerozoic time. In: Sloss, L.L. (Ed.), The Geology of North America, v. D-2, Sedimentary Cover–North American Craton: U.S., (Vol. D-2). Geological Society of America, Boulder, CO, pp. 25–51.
- Stanley, J.R., Flowers, R.M., Bell, D.R., 2015. Erosion patterns andmantle sources of topographic change across the southern African Plateau derived from the shallow and deep records of kimberlites. Geochem. Geophys. Geosyst. 16, 3235–3256. https://doi.org/10.1002/2015GC005969.
- Stanley, J.R., Braun, J., Baby, G., Guillocheau, F., Robin, C., Flowers, R.M., et al., 2021. Constraining Plateau Uplift in Southern Africa by combining thermochronology, sediment flux, topography, and landscape evolution modeling. J. Geophys. Res., Solid Earth 126 (7), 1–34. https://doi.org/10.1029/2020JB021243.
- Sturrock, C.P., Flowers, R.M., Macdonald, F.A., 2021. The late great unconformity of the Central Canadian Shield. Geochem. Geophys. Geosyst. 22 (6), 1–22. https:// doi.org/10.1029/2020GC009567.
- Swanson-Hysell, N.L., Burgess, S.D., Maloof, A.C., Bowring, S.A., 2014. Magmatic activity and plate motion during the latent stage of Midcontinent Rift development. Geology 42 (6), 475–478. https://doi.org/10.1130/G35271.1.
- Tegner, C., Andersen, T.B., Kjøll, H.J., Brown, E.L., Hagen-Peter, G., Corfu, F., et al., 2019. A mantle plume origin for the Scandinavian dyke complex: a "piercing point" for 615 Ma plate reconstruction of Baltica? Geochem. Geophys. Geosyst. 20 (2), 1075–1094. https://doi.org/10.1029/2018GC007941.
- Tinker, J., de Wit, M., Brown, R., 2008. Mesozoic exhumation of the southern Cape, South Africa, quantified using apatite fission track thermochronology. Tectonophysics 455 (1–4), 77–93. https://doi.org/10.1016/j.tecto.2007.10.009.
- Zotto, S.C., Moecher, D.P., Niemi, N.A., Thigpen, J.R., Samson, S.D., 2020. Persistence of Grenvillian dominance in Laurentian detrital zircon age systematics explained by sedimentary recycling: evidence from detrital zircon double dating and detrital monazite textures and geochronology. Geology 48 (8), 792–797. https:// doi.org/10.1130/G47530.1.